Comparison of physicochemical properties and selective catalytic reduction activities of CeMn/TiO_2 catalysts with and without phosphorus additives

Zeycan KESKİN (zeycankeskin01@gmail.com)
Republic of Turkey Ministry of National Education: Turkiye Cumhuriyeti Milli Egitim Bakanligi
https://orcid.org/0000-0003-1812-8742

Research Article

Keywords: Characterization, Catalyst deactivation, Nitrogen oxides, Phosphorus poisoning, Selective catalytic reduction

Posted Date: August 12th, 2021

DOI: https://doi.org/10.21203/rs.3.rs-749508/v1

Version of Record: A version of this preprint was published at International Journal of Automotive Science And Technology on November 10th, 2021. See the published version at https://doi.org/10.30939/ijastech..1003870.

Abstract

Lubricant additives contain phosphorus, which has a fly ash effect. Phosphorus negatively affects catalyst activity. Determining the effects of phosphorus loading amount on the catalytic activity is important for the development of catalysts with high NO_x reduction.

This study focuses on the control of NO_x emissions, one of the air pollutants released from the diesel engine. The catalysts used in the reduction of NO_x emissions were synthesized by washcoating method. Ce and Mn contents of all catalysts were adjusted as 3%, while the phosphorus contents of poisoned catalysts were adjusted as 0.5% and 1%. For this purpose, cordierite with high surface area was used. The catalysts were characterized by scanning electron microscopy (SEM), energy dispersive spectroscopy (EDS), Brunauer-Emmett-Teller (BET), X-Ray diffraction (XRD) and ultraviolet visible spectroscopy (UV-Vis) analyzes. The NO_x reduction activity of with and without phosphorus doped $CeMn/TiO_2$ catalysts was investigated with the designed selective catalytic reduction system (SCR).

NO_x conversion ratios of the $CeMn/TiO_2$ catalyst reached the high values of 84.6% at 280°C. After the phosphorus loading, the structure of the $CeMn/TiO_2$ catalyst deteriorated, and the NO_x conversion ratios decreased. $0.5P\text{-}CeMn/TiO_2$ and $1P\text{-}CeMn/TiO_2$ catalysts showed lower NO_x conversion ratios compared to $CeMn/TiO_2$ catalyst.

$CeMn\text{-}TiO_2$ catalyst was found highly active for SCR at all tests. Phosphorus loading caused deactivation of the catalyst and deactivation increased due to the increase in phosphorus loading amount.

1. Introduction

Nitrogen oxides (NO_x), which are mostly released from diesel emissions, cause severe air pollutions such as acid rain, ozone depletion. Recently, many countries have been reinforced regulations for removing NO_x emissions. Therefore, many aftertreatment technologies have been developed for emission control. The most effective method for NO_x removal is the selective catalytic reduction (SCR) system. (Zhang and Zhong, 2015; Reşitoğlu et al. 2015; Ma et al. 2020).

Different reductants such as H_2, CO, ammonia, urea, hydrocarbons are used to react with NOx in SCR system (Valanidou et al. 2011; Väliheikki et al. 2014). The SCR technology with hydrocarbons as a reductant (HC-SCR) is promising as an alternative to other reductants due to its advantages (More et al. 2015).

Active catalysts for HC-SCR at low temperature conditions are important. Until now, many SCR catalysts have been developed for NO_x reduction under different conditions. A manganese oxide (MnO_x) SCR catalyst has been widely used for NO_x removal because of its low cost, high thermal stability and higher SCR activity than other catalysts at low temperatures (Xu et al. 2013). However, as MnO_x loading amount increases agglomeration increases and MnO_x is not dispersed perfectly on the catalyst surface (Liu et al.

2016). Liu et al. (2016) found that Mn-Ni/OMA exhibits higher NO_x conversion performance than Mn-Ni/γ-Al_2O_3 in the 90–240°C temperature window. Guo et al. (2019) revealed that Mn-Eu-Fe catalyst with Fe/Mn molar ratio of 1 and calcination temperature of 500°C has the highest SCR activity with 98% NO conversion at 100°C using NH_3 reductant.

Among transition metal catalysts, cerium oxide (CeO_2) catalysts exhibit potential advantages such as high oxygen storage capacity, strong interaction with metals (Zeng et al. 2020). Moreover, CeO_2 shows good catalytic activity in the SCR system at low temperatures. Han et al. (2019) proved that Ce doped Mn-Fe/Al_2O_3/CC catalyst exhibited higher activity than W, Cu, Co doped catalysts. The maximum NO conversion ratio of Mn-Fe-Ce/Al_2O_3/CC catalyst was 72% at 250°C and 5971 h^{-1}. Chen et al. (2021) synthesized Mn-Ce mixed-oxide catalyst exhibiting good low temperature activity. They achieved above 90% NO_x conversion in the temperature of 150–310 ℃ with this catalyst.

Catalysts may be deactivated due to the use of lubricating additives such as detergents, dispersants and viscosity improvers in vehicles (Kröcher and Elsener, 2008; Albert et al. 2019). These additives convert to inorganic compounds and emit into the exhaust gas (Kröcher and Elsener, 2008). Lubricating oil additives contain calcium, sulfur, zinc and phosphorus are which often present in forms $CaCO_3$ (or CaO), SO_2, ZnO and H_3PO_4 (Wang et al. 2018). These inorganic deposits are chemically absorbed on the active sites of the catalyst, causing pores blockage and surface loss. This might lead to the poisoning of SCR catalysts, and catalyst poisoning is the major reason for catalyst deactivation (Chen et al. 2018; Qi et al. 2019). However, it is important that the tolerance of SCR catalysts to chemical poisoning is maintained throughout the lifetime of the vehicle (Kröcher and Elsener, 2008; Chen et al. 2018).

In recent years, the effect of catalyst poisoning has been studied by some research groups. Wei et al. (2018) investigated the poisoning effect on activity of Mn/TiO_2 catalyst. They found the potassium species have a negative impact on Mn/TiO_2 catalytic activity. Xie et al. (2019) studied the deactivation of Cu-SSZ-13 SCR catalysts with vapor-phase phosphorus and reported that the deactivation degrees were proportional to the P/Cu ratio. You et al. (2017) investigated the poisoning effects of phosphorus on CeO_2-MoO_3/TiO_2 catalysts in selective catalytic reduction of NO_x with NH_3. They found that the chemical deactivation effects of phosphorus resulted from decreases in the number of active sites and in the adsorption capacity for NO_x species. That exposure of Fe-zeolite catalysts to phosphates leads to deactivation of the catalyst was detected by Kern et al. (2010) Gong et al. (2020) researched the P_x-$Ce_{0.3}$-Zr-Ti catalysts prepared by hydrothermal method and the effect of P modification on NH_3-SCR property and structure. The results showed that adding appropriate amount of $H_4P_2O_7$ increased the specific surface area of catalysts and provided more reaction sites for active gases.

As there are always traces of inorganic compounds in the exhaust, it is important to understand their effect on the catalytic performance. There are not enough studies concerning the impact of inorganic poisons on the performance of OHC-SCR catalysts in the literature. In this study, to investigate the

phosphorus deactivation effects on CeMn/TiO_2 catalysts, phosphorus doped catalysts with different contents were prepared and SCR activities were compared.

2. Materials And Methods

2.1. Catalyst synthesis and characterization

2.1.1. Catalyst synthesis

In this study, ceramic monoliths with a honeycomb structure of cordierite ($2Al_2O_3.5SiO_2.2MgO$) were used as catalyst support with a volume of 200 cm^3. However, the surface area of honeycomb cordierite is very low, as 1 m^2/g, and difficult to load active components directly (Shigapov et al. 1999; Lu et al. 2017; Li et al. 2016). Shigapov et al. (1999) reported that oxalic acid has relatively low volatility in aqueous solution, is less destructive and improves surface area of cordierite. Therefore, it was pre-treated with 50% hot oxalic acid solution for 3 hours to increase the surface area of the cordierite samples. After 3 hours, samples were washed with deionized water until the washing liquid pH value was 7.0. Then, they were dried at 110 ^oC for 1 hour in the oven, calcined at 500 ^oC for 3 hours in the muffle furnace and prepared for coating.

A powder catalyst was prepared to synthesize the SCR catalyst by the washcoating method for this study. The Ce and Mn content of the catalysts were set at 3 wt%. The required amount of cerium (III) acetate hydrate (99.9%, $Ce(CH_3CO_2)_3 \cdot xH_2O$) and manganese (IV) oxide (≥ 90%, MnO_2) as precursors were initially dissolved in 500 mL deionized water and stirred for 30 min with ultrasonic vibration. 94 wt% titanium (IV) oxide (≥ 99%, TiO_2) was then added to solution and continuously stirred for 30 min. TiO_2 was used to improve the surface area of cordierite and to provide active sites for reduction reactions. The obtained solution was mixed with a rotary evaporator and was heated. This process was continued until the excess water in the solution was removed. The resulting solution was dried at 120 ^oC for 2 hours in the oven and was calcined at 500 ^oC for 3 hours in the muffle furnace. After milling, the catalyst powder was obtained.

The catalyst powder was used for the washcoating of pre-treated cordierite monoliths. Prior to the washcoating, 40g catalyst powder was added to deionized water and was stirred for 1 hour by ultrasonic vibration.

The pre-treated cordierite substrate with volume of 200 cm^3 were dipped in the slurry and excess slurry was removed. Then, catalyst was dried in the oven for 1 hour at 120 ^oC. The washcoated substrate was finally calcined in the muffle furnace at 500 ^oC for 3 hours and was labelled as CeMn/TiO_2.

2.1.2. Preparation of poisoned catalysts

Two powder catalyst slurry samples were prepared using 40g of catalyst powder to make poisoned catalysts. Then, the desired amounts of P (from ammonium phosphate, $NH_4H_2PO_4$) elements addition in the slurries were made. The content of P added to the catalyst was set at 0.5 wt% and 1 wt%. The slurries were stirred at room temperature for 1 hour. After dipping, the samples were dried at 120°C for 1 hour and were calcined at 500°C for 3 hours.According to added P element mass, the poisoned samples were labelled as 0.5P-CeMn/TiO_2 (0.5 wt% P), 1P-CeMn/TiO_2 (1 wt% P).

2.1.3. Catalysts characterization

Morphologies and structural features of samples were investigated by scanning electron microscopy (SEM) using FEI Quante 650 FEG scanning electron microscope. Energy Dispersive Spectroscopy (EDS) analysis was used to the dispersion of catalytic elements and semi quantitative determination of elements ratio in the particular area of catalysts.

The specific surface area, pore volume and pore area of samples were measured with a Sorptometer 1042 apparatus using physical adsorption method of N_2. The samples were degassed at 200 ^oC for 60 min prior to measurements. The Brunauer-Emmett-Teller (BET) method was used to determine the specific surface area and Barrett-Joiner-Halenda (BJH) method was used to determine the pore size distribution.

The X-Ray Diffraction (XRD) was used to establish the crystallographic phase information of catalysts. The patterns were collected using a PANalytical Empyrean diffractometer in the 2 θ range of 10–90 ^{o}.

An ultraviolet visible (UV-vis) spectroscopy analysis of samples was recorded at room temperature using an Agilent Cary 7000 Universal Measurement Spectrophotometer in the wavelength range of 190–1100 nm.

2.2. Catalytic performance test system

The activity of the catalysts was investigated under real conditions and the tests were carried out at temperatures between 200 and 280°C. The NO_x removing efficiency of the CeMn/TiO_2, 0.5P-CeMn/TiO_2 and 1P-CeMn/TiO_2 catalysts were evaluated using a performance test system at different engine loads with ethanol reductant. A test system consisting of many parts was designed for performance tests. Schematic diagram of performance test system was given in Fig. 1.

Two cylinders, 830 cm^3 cylinder volume, 79 mm stroke, 80 mm bore, 3000 rpm engine speed and 23/1 compression ratio, AKSA A2CRX08 model diesel engine was used to exhaust gas samples. Flow rate of the test system was maintained at 30000 h^{-1} gas hourly space velocity (GHSV) by an orifice plate, whose pressure was controlled with a digital and a U manometer. The aftertreatment system included a diesel oxidation catalyst (DOC) and a SCR catalyst for different experiments. Two Continental UniNO_x sensors were used to measure the NO_x concentrations before and after SCRs. The exhaust gas temperatures of critical points inside the engine after DOC and before SCR were monitored by two K type thermocouple

temperature sensors. Controlled using an electric pump and a multipoint electro-hydraulic injector, the mixing chamber was placed between the SCR and DOC to inject the reductant.

The exhaust gas compositions of the test system at 0 kW, 1 kW, 2 kW and 3 kW engine loads were given in Table 1. HC emission concentrations remained at 63–64 ppm for different loads, while NO_x emission concentrations increased from 184 to 380 ppm.

Table 1
Engine exhaust gas composition without exhaust emission control system at different loads

Emission values	0 kW	1 kW	2 kW	3 kW
NO_x (ppm)	184	263	344	387
O_2 (%)	15.75	14.93	14.14	13.73
CO (%)	0.061	0.048	0.039	0.033
C_xH_y (ppm)	64	64	63	63

3. Results And Discussion

3.1. NO_x conversion performances of catalysts

The operating temperature range of the tests conducted to investigate the catalytic activity was between 200 and 280°C. The results of tests performed to investigate the effect of phosphorus on the activity of the $CeMn/TiO_2$ catalyst were shown in Fig. 2.

It was observed that the activity of all catalysts increased depending on the temperature increase. Maximum NO_x conversion ratios of $CeMn/TiO_2$, $0.5P\text{-}CeMn/TiO_2$ and $1P\text{-}CeMn/TiO_2$ catalysts at 280°C were 84.6%, 80.3% and 78.5%, respectively. In our previous studies, we proved that the positive effect of temperature increases on catalytic activity (Keskin[a], 2021; Keskin et al. 2021; Keskin[b], 2021). The lowest NO_x conversion ratios were obtained at 200°C and were 67.8%, 67.5% and 64.5% for the $CeMn/TiO_2$, $0.5P\text{-}CeMn/TiO_2$ and $1P\text{-}CeMn/TiO_2$ catalysts, respectively.

Previous research has shown that phosphorus leads to a decrease in catalytic activity due to its negative effect on the chemical properties of the catalyst. You et al. (2017) found that the CeMo/Ti catalyst exhibited 100% NO conversion at 400°C, whereas the 1.32P-CeMo/Ti catalyst showed 57% NO conversion. Chen et al. (2018) proved that the NO conversion of Cu-S catalyst was 83% at 250 ℃, while the NO conversions of 0.1, 0.2 and 0.4 P loaded Cu-S catalysts were 73%, 65% and 45%, respectively.

It was observed that the NO_x conversion of the $CeMn/TiO_2$ and $0.5P\text{-}CeMn/TiO_2$ catalysts at low temperatures was close. However, the increase in $CeMn/TiO_2$ catalyst activity was greater with the

increase in temperature. It was determined that the 1P-CeMn/TiO_2 catalyst activity was lower than the activity of other catalysts at all temperatures. In the tests, it was seen that phosphorus negatively affected the catalytic activity. As the phosphorus content in the catalyst increased, the catalyst activity decreased significantly. The decrease in NO_x conversion ratios of poisoned catalysts was higher at temperatures between 240 and 280°C. When the NO_x conversion ratios of the CeMn/TiO_2 and the poisoned catalysts were compared at 280°C and 1 kW engine load, the decrease in the NO_x conversion ratio for the 0.5P-CeMn/TiO_2 and 1P-CeMn/TiO_2 catalysts was 5.4% and 8.9%, respectively. The results proved that the increase in the catalysts' phosphorus content remarkably affects the catalytic activity.

When the NO_x conversion ratios at 1 kW and 3 kW engine loads were compared, a difference was found approximately 1.3% with CeMn/TiO_2 catalyst, 1.1% with 0.5P-CeMn/TiO_2 catalyst, and 1.5% with 1P-CeMn/TiO_2 catalyst. It was seen that the difference in NO_x conversion ratios obtained at different engine loads was not much. As a result, it was concluded that the catalysts maintain their activity at all engine loads and the catalyst production method was successful. Although the difference between the two engine loads is not much, it was seen that the increase in engine load caused an increase in catalytic activity and higher NO_x conversion ratios were obtained at 3 kW engine load. As can be seen in Table 1, the oxygen concentration decreased due to the increase in engine loads. The reason for this was thought that the decrease in oxygen concentration due to the increase in engine load and the decrease in the effect of DOC. Similar results were also found by researchers (Keskin[b], 2021 Ahmad et al. 2020; Yaşar et al. 2019).

3.2. Characterization of catalysts

The surface morphology and structure of the fresh catalyst and poisoned catalysts were observed by SEM analysis. SEM images of CeMn/TiO_2, 0.5P-CeMn/TiO_2 and 1P-CeMn/TiO_2 catalysts at 10000 times magnification were shown in Fig. 3. SEM images showed that the particles were very small size and were homogeneously dispersed over the both pores and also surface of the catalysts. The crystallization in both fresh and also poisoned catalysts was seen. It could be considered that this crystallization is the result of the calcination of catalytic elements. As seen in Fig. 3, the crystallization of the poisoned catalysts was affected by the phosphorus ratios and increased on the 1P-CeMn/TiO_2 catalyst. The homogeneous distribution in small particles has an increasing effect on the catalytic activity. For this reason, the activity of 1P-CeMn/TiO_2 catalyst may have been lower than other catalysts. In addition, pores of the 1P-CeMn/TiO_2 catalyst were not as clear as other catalysts. It was thought that some pores were blocked by the phosphorus elements. The decrease in catalytic activity may be due to pores blockage.

The EDX mapping was performed to examine the distributions of elements on the catalysts and was shown in Fig. 4. Oxygen, magnesium, aluminum and silicon were present in all catalysts. These elements existed the structure of cordierite, which is used as the main material in catalyst synthesis. The TiO_2 compounds show both catalytic effect and increase the surface area. Therefore, its distribution on the

surface significantly affects the catalytic activity. In EDX mapping, it was seen that TiO_2 had the highest ratio in all catalysts. However, the increase in the amount of phosphorus negatively affected the distribution of TiO_2 on the catalyst surface. The reduction of TiO_2 on the surface of the 1P-CeMn/TiO_2 catalyst may have caused the decrease catalytic activity.
It was observed that cerium and manganese elements, which showed catalytic effects, showed good distribution in all catalysts. With EDX mappings, it was proven that phosphorus exists in poisoned catalysts and therefore reduces the catalytic effect.

The surface area has a significant effect on catalytic activity. Therefore, surface area analyzes of the catalysts were performed and the BET surface area and micropore volumes of the catalysts were given in Table 2. According to BET results, the surface area of CeMn/TiO_2 catalyst was 25.55 m^2/g and had the highest surface area. The surface area of the catalysts containing phosphorus was lower and the surface area decreased further as the phosphorus loading ratio increased. The reduction in the surface area of the 0.5P-CeMn/TiO_2 catalyst was 47.2% while it was 51.7% for the 1P-CeMn/TiO_2 catalyst. The reduction in surface area is one of the reasons for the reduced NO_x conversion ratios of poisoned catalysts. Because the regions where NO_x reduction reactions take place on the surface decreased. When the micropore volumes were compared, it was seen that the micropore volumes of the phosphorus containing catalysts were lower and these results were compatible with the SEM images. It is known that an increase in micropore volume positively affects catalytic activity. The best activity of the CeMn/TiO_2 catalyst can be due to the higher surface and micropores volume than other catalysts.

Table 2
BET surface area and micropore volume of catalysts

	CeMn/TiO_2	0.5P-CeMn/TiO_2	1P-CeMn/TiO_2
BET surface area (m^2/g)	25.55	13.48	12.33
Micropore volume (mm^3/g)	6.03	4.6	2.28

The crystal structure of catalytic elements on the surface provides information about the catalyst activity. Therefore, XRD analysis was performed and results were presented in Fig. 5. The results of the analysis indicated that cordierite has the highest intensity peaks on the catalysts due to its use as the main structure. Peaks at 2θ = 10.42 °, 26.35 °, 29.43 ° were associated with the cordierite. It was seen that the catalytic elements were contributed to the crystal structure. The peaks at 2θ = 21.8 ° and 2θ = 28.1 ° were associated with MnO_2 and CeO_2, respectively. After phosphorus addition observed no difference in the shape and intensity of these peaks. The catalytic activities of the catalysts were close to each other, especially at 200°C, which could be attributed to the fact that the peak intensity of the cerium and manganese does not change. As can be seen in Fig. 5, no peaks of TiO_2 were found. The no visible TiO_2 peaks may have been due to their very good surface distribution or strong interaction with the coating

elements. These results were consistent with EDX analysis. Phosphorus peaks were observed on 0.5P-CeMn/TiO_2 and 1P-CeMn/TiO_2 catalysts at 2θ = 35 °. It was concluded that the activity of the poisoned catalysts was lower than the CeMn/TiO_2 catalyst due to the phosphorus element. In addition, the increase in the intensity of the phosphorus peaks with increasing phosphorus content explained that 0.5P-CeMn/TiO_2 catalyst activity was higher than the 1P-CeMn/TiO_2 catalyst activity.

The chemical state of catalytic element species was examined with UV-Vis spectra and results were shown in Fig. 6. The chemical state of catalytic elements plays an important role in catalytic reductions. It was observed that all catalysts showed intense absorption bands and the absorption edges were noticeable. TiO_2 provides active sites for NO_x reduction, thus increasing catalytic activity. The characteristic strong absorption bands were observed at approximately 380 nm, which is compatible with anatase TiO_2 (Tian et al. 2015). The intensity of the adsorption band of TiO_2 did not change in all catalysts. According to previous studies (Chen et al. 2019; Gupta et al. 2017) the bands at 340–400 nm can be attributed to CeO_2 and absorption band at 316 nm, corresponded to MnO_2.

The absorption band intensity of poisoned catalysts with an increase of phosphorus loading was not changed. However, a big difference was seen between the CeMn/TiO_2 and poisoned catalysts in the range between 260 and 320 nm. Obvious changes were observed after the phosphorus was added to the catalyst, proving that phosphorus significantly affects the activity. 0.5P-CeMn/TiO_2 and 1P-CeMn/TiO_2 catalysts showed a higher absorption from 470 nm to 710 nm than CeMn/TiO_2 catalyst, indicating that the absorption increases with the increase of the wavelength. Agglomeration of catalytic elements during sintering can affect catalytic activity. The absorption band increases as increase in wavelength due to aggregation in the UV spectrum. In 0.5P-CeMn/TiO_2 and 1P-CeMn/TiO_2 catalysts, it was thought that increase in the absorption band intensity at 470–710 nm wavelength range might be due to agglomeration. These results supported the reduction in the catalytic activity of the poisoned catalysts.

4. Conclusions

Fresh and poisoned catalysts showed > 70% NO_x conversion ratio at 280°C. The significant diversity was detected in fresh and poisoned catalyst activity for NO_x reduction using ethanol reductant. The performance of the CeMn/TiO_2 catalyst was highest at all test temperatures. The NO_x reduction performance of CeMn/TiO_2 catalyst was affected by the phosphorus loading content. The catalyst was deactivated by phosphorus loading and SCR activity further decreased after phosphorus loading increased. The SCR activity of 0.5 P-CeMn/TiO_2 catalyst was higher compared to the 1P-CeMn/TiO_2 catalyst. The increased engine load was favorable for NO_x conversions because the oxygen concentration which caused the DOC ineffective was reduced. However, the increase was not significant, indicating high catalyst stability. The higher activity of CeMn/TiO_2 catalyst was associated with small and well dispersed particles, high surface area and micropore volume, and was confirmed by SEM, EDX

and BET analyzes. XRD and UV-Vis spectrum revealed surface change and agglomeration leading to lower activity of poisoned catalysts.

Declarations

Author Contributions Zeycan Keskin contributed to the conception and design of the study. Material preparation, data collection and analysis were performed by Zeycan Keskin. The first draft of the manuscript was written and commented by Zeycan Keskin. The author read and approved the final manuscript.

Funding No funding was obtained for this study.

Data Availability The data sets generated and/or analyzed during the current study are available from the corresponding author on reasonable request.

Code Availability Not applicable.

Declarations The work is original and not published elsewhere.

Conflicts of Interest/Competing Interests The author declares that there is no conflict of interest.

Ethics Approval The manuscript was not submitted to more than one journal for simultaneous consideration.

References

1. Albert KB, Fan C, Pang L, Chen Z, Ming S, Albert T, Li T (2019) The influence of chemical poisoning, hydrothermal aging and their co-effects on Cu-SAPO-34 catalyst for NO_x reduction by NH_3-SCR. Appl Surf Sci 479:1200–1211. https://doi.org/10.1016/j.apsusc.2019.02.120.
2. Ahmad MACM, Keskin A, Özarslan H, Keskin Z (2020) Properties of ethyl alcohol-water mixtures as a reductant in a SCR system at low exhaust gas temperatures. Energy Sources, Part A. InPress. 1556–7230. https://doi.org/10.1080/15567036.2020.1733142
3. Chen Z, Fan C, Pang L, Ming S, Liu P, Li T (2018) The influence of phosphorus on the catalytic properties, durability, sulfur resistance and kinetics of Cu-SSZ-13 for NO_x reduction by NH_3-SCR. Appl Catal B: Environ 237:116–127. https://doi.org/10.1016/j.apcatb.2018.05.075.
4. Chen L, Wang X, Cong Q, Ma H, Li S, Li W (2019) Design of a hierarchical Fe-ZSM-5@CeO_2 catalyst and the enhanced performances for the selective catalytic reduction of NO with NH_3. Chem Eng J 369:957–967. https://doi.org/10.1016/j.cej.2019.03.055
5. Chen JY, Fu P, Lv D, Chen Y, Fan M, Wu J, Meshram A, Mu B, Li X, Xia Q (2021) Unusual positive effect of SO_2 on Mn-Ce Mixed-Oxide Catalyst for the SCR reaction of NO_x with NH_3. Chem Eng J 407:127071. https://doi.org/10.1016/j.cej.2020.127071

6. Gong P, Xie J, Fang D, He F, Li F, Qi, K (2020) Enhancement of the NH_3-SCR property of Ce-Zr-Ti by surface and structure modification with P. Appl Surf Sci 505:144641. https://doi.org/10.1016/j.apsusc.2019.144641.
7. Guo M, Zhao P, Liu Q, Liu C, Han J, Ji N, Song C, Ma D, Lu X, Liang X, Li Z (2019) Improved low-temperature activity and H_2O resistance of Fe doped Mn-Eu catalysts for NO removal by NH_3-SCR. ChemCatChem 11(19):4954–4965. https://doi.org/10.1002/cctc.201900979
8. Gupta VK, Fakhri A, Agarwal S, Sadeghi N (2017) Synthesis of MnO_2/cellulose fiber nanocomposites for rapid adsorption of insecticide compound and optimization by response surface methodology. Int J Biol Macromol 102:840–846. https://doi.org/10.1016/j.ijbiomac.2017.04.075
9. Han W, Yi H, Tang X, Zhao S, Gao F, Zhang X, Ma C, Song L (2019) Mn-Fe-Ce coating onto cordierite monoliths as structured catalysts for NO catalytic oxidation. ChemistrySelect 4:4664–4671. https://doi.org/10.1002/slct.201900834
10. Kern P, Klimczak M, Heinzelmann T, Lucas M, Claus P (2010) High-throughput study of the effects of inorganic additives and poisons on NH_3-SCR catalysts. Part II: Fe–zeolite catalysts. Appl Catal B: Environ 95:48–56. https://doi.org/10.1016/j.apcatb.2009.12.008.
11. Keskin[a] Z (2021) Enhancing of low-temperature OHC-SCR activity of Ag/TiO_2 with addition of MnO_2 nanoparticles, and performance evaluation using diesel engine exhaust gases. Environ Technol Innov 21:101205. https://doi.org/10.1016/j.eti.2020.101205.
12. Keskin Z, Özgür T, Özarslan H, Yakaryılmaz AC (2021) Effects of hydrogen addition into liquefied petroleum gas reductant on the activity of Ag-Ti-Cu/Cordierite catalyst for selective catalytic reduction system. Int J Hydrogen Energy46:7637641.https://doi.org/10.1016/j.ijhydene.2020.11.200.
13. Keskin[b] Z (2021) Investigation of deactivation effect of Au addition to Ce/TiO_2 catalyst for selective catalytic reduction using real diesel engine exhaust samples at low temperature conditions. J Chem Technol Biotechnol 96 (8), 2275–2282. DOI 10.1002/jctb.6753.
14. Kröcher O, Elsener M (2008) Chemical deactivation of V_2O_5/WO_3–TiO_2 SCR catalysts by additives and impurities from fuels, lubrication oils, and urea solution I. Catalytic studies. Appl Catal B: Environ 75:215–227. https://doi.org/10.1016/j.apcatb.2007.04.021.
15. Li F, Shen B, Tian L, Li G, He C (2016) Enhancement of SCR activity and mechanical stability on cordierite supported V_2O_5-WO_3/TiO_2 catalyst by substrate acid pretreatment and addition of silica, Powder Technol 297:384–391. https://doi.org/10.1016/j.powtec.2016.04.050.
16. Liu Y, Hou Y, Han X, Wang J, Guo Y, Xiang N, Bai Y, Huang Z (2016) Effect of ordered mesoporous alumina support on the structural and catalytic properties of Mn-Ni/OMA catalyst for NH_3-SCR performance at low-temperature. ChemCatChem 12(3):953–962. https://doi.org/10.1002/cctc.201901466
17. Lu S, Zhang J, Sun Y, Liu H (2017) Preparation and characterization of CuO-CeO_2-ZrO_2/cordierite monolith catalysts. Ceram Int 43:5957–5962. https://doi.org/10.1016/j.ceramint.2017.01.118

18. Ma S, Tan H, Li Y, Wang P, Zhao C, Niu X, Zhu Y (2020) Excellent low-temperature NH_3-SCR NO removal performance and enhanced H_2O resistance by Ce addition over the $Cu_{0.02}Fe_{0.2}Ce_yTi_{1-y}O_x$ (y = 0.1, 0.2, 0.3) catalysts. Chemosphere. 243:125309. https://doi.org/10.1016/j.chemosphere.2019.125309.
19. More PM, Nguyen DL, Granger P, Dujardin C, Dongare MK, Umbarkar SB (2015) Activation by pretreatment of Ag-Au/Al_2O_3 bimetallic catalyst to improve low temperature HC-SCR of NO_x for lean burn engine exhaust. Appl Catal B: Environ. 174–175:145–156. https://doi.org/10.1016/j.apcatb.2015.02.035.
20. Qi L, Li J, Yao Y, Zhang Y (2019) Heavy metal poisoned and regeneration of selective catalytic reduction catalysts. J Hazard Mater. 366:492–500. https://doi.org/10.1016/j.jhazmat.2018.11.112.
21. Reşitoğlu İA, Altinişik K, Keskin A (2015) The pollutant emissions from diesel-engine vehicles and exhaust aftertreatment systems. Clean Techn. Environ. Policy. 17:15–27. DOI 10.1007/s10098-014-0793-9.
22. Shigapov AN, Graham GW, McCabe RW, Peck MP, Plummer HK (1999) The preparation of high-surface-area cordierite monolith by acid treatment, Appl. Catal. A.: Gen. 182:137–146. https://doi.org/10.1016/S0926-860X(99)00003-4.
23. Tian J, Leng Y, Zhao Z, Xia Y, Sang Y, Hao P, Zhan J, Li M, Liu H (2015) Carbon quantum dots/hydrogenated TiO_2 nanobelt heterostructures and their broad spectrum photocatalytic properties under UV, visible, and near-infrared irradiation. Nano Energy. 11:419–427. https://doi.org/10.1016/j.nanoen.2014.10.025
24. Valanidou L, Theologides C, Zorpas AA, Savva PG, Costa CN (2011) A novel highly selective and stable Ag/MgO-CeO_2-Al_2O_3 catalyst for the low-temperature ethanol-SCR of NO. Appl Catal B: Environ. 107:164–176. https://doi.org/10.1016/j.apcatb.2011.07.010.
25. Väliheikki A, Petallidou KC, Kalamaras CM, Kolli T, Huuhtanen M, Maunula T, Keiski RL, Efstathiou AM (2014) Selective catalytic reduction of NO_x by Hydrogen (H_2-SCR) on WO_x-promoted $Ce_2Zr_{1-Z}O_2$ solids. Appl Catal B: Environ 156–157:72–83. https://doi.org/10.1016/j.apcatb.2014.03.008.
26. Wang P, Chen S, Gao S, Zhang J, Wang H, Wu Z (2018) Niobium oxide confined by ceria nanotubes as a novel SCR catalyst with excellent resistance to potassium, phosphorus, and lead. Appl Catal B: Environ 231:299–309. https://doi.org/10.1016/j.apcatb.2018.03.024.
27. Wei L, Cui S, Guo H, Zhang L (2018) The effect of alkali metal over Mn/TiO_2 for low-temperature SCR of NO with NH_3 through DRIFT and DFT. Comput Mater Sci 144:216–222. https://doi.org/10.1016/j.commatsci.2017.12.013.
28. Xie K, Wang A, Woo J, Kumar A, Kamasamudram K, Olsson L (2019) Deactivation of Cu-SSZ-13 SCR catalysts by vapor-phase phosphorus exposure. Appl Catal B: Environ 256:117815. https://doi.org/10.1016/j.apcatb.2019.117815.
29. Xu L, Li XS, Crocker M, Zhang ZS, Zhu AM, Shi C (2013) A study of the mechanism of low-temperature SCR of NO with NH_3 on MnO_x/CeO_2. J Mol Catal A Chem 378:82–90.

https://doi.org/10.1016/j.molcata.2013.05.021.

30. Yaşar A, Keskin A, Keskin Z, Özarslan H, Kaltar S (2019) Low temperature catalytic activity of Ag based SCR catalysts with 2-propanol—toluene mixture as reductant. Mater Res Express 6:095523. https://doi.org/10.1088/2053-1591/ab31ea
31. You Y, Chang H, Zhu T, Zhang T, Li X, Li J (2017) The poisoning effects of phosphorus on CeO_2-MoO_3/TiO_2 $DeNO_x$ catalysts: NH_3-SCR activity and the formation of N_2O. Mol Catal 439:15–24. https://doi.org/10.1016/j.mcat.2017.06.013.
32. Zhang S, Zhong Q (2015) Surface characterization studies on the interaction of V_2O_5–WO_3/TiO_2 catalyst for low temperature SCR of NO with NH_3. J Solid State Chem 221:49–56. https://doi.org/10.1016/j.jssc.2014.09.008.
33. Zeng Y, Haw KG, Wang Y, Zhang S, Wang Z, Zhong Q, Kawi S (2020) Recent progress of CeO_2-TiO_2 based catalysts for selective catalytic reduction of NO_x by NH_3. ChemCatChem 13(2):491–505. https://doi.org/10.1002/cctc.202001307

Figures

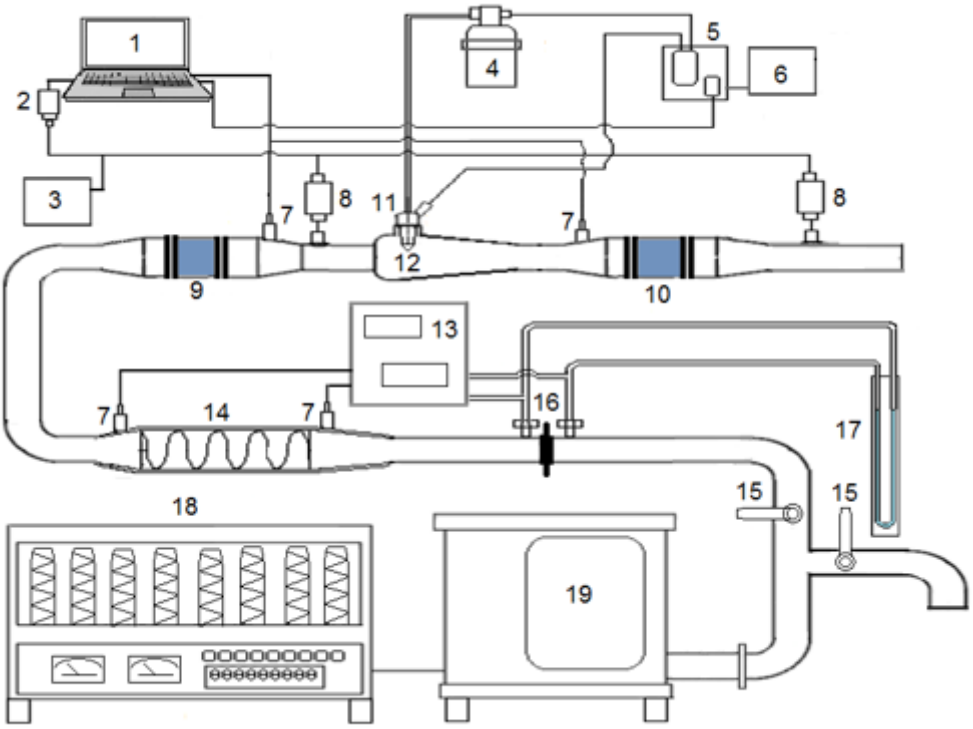

Figure 1

Schematic diagram of performance test system (1-Computer, 2- PEAK 3- 24V power supply, 4- Pump and reductant tank, 5- Microprocessor, 6- 12V power supply, 7- Temperature sensor, 8- NOx sensor, 9- DOC(Diesel oxidation catalyst), 10- SCR catalyst, 11- Injector, 12- Mixture chamber, 13- Digital manometer

and exhaust gas heater system control unit, 14 - Exhaust gas heater, 15- Valve, 16- Orifice plate, 17- U manometer, 18- Loading system 19- Diesel Engine

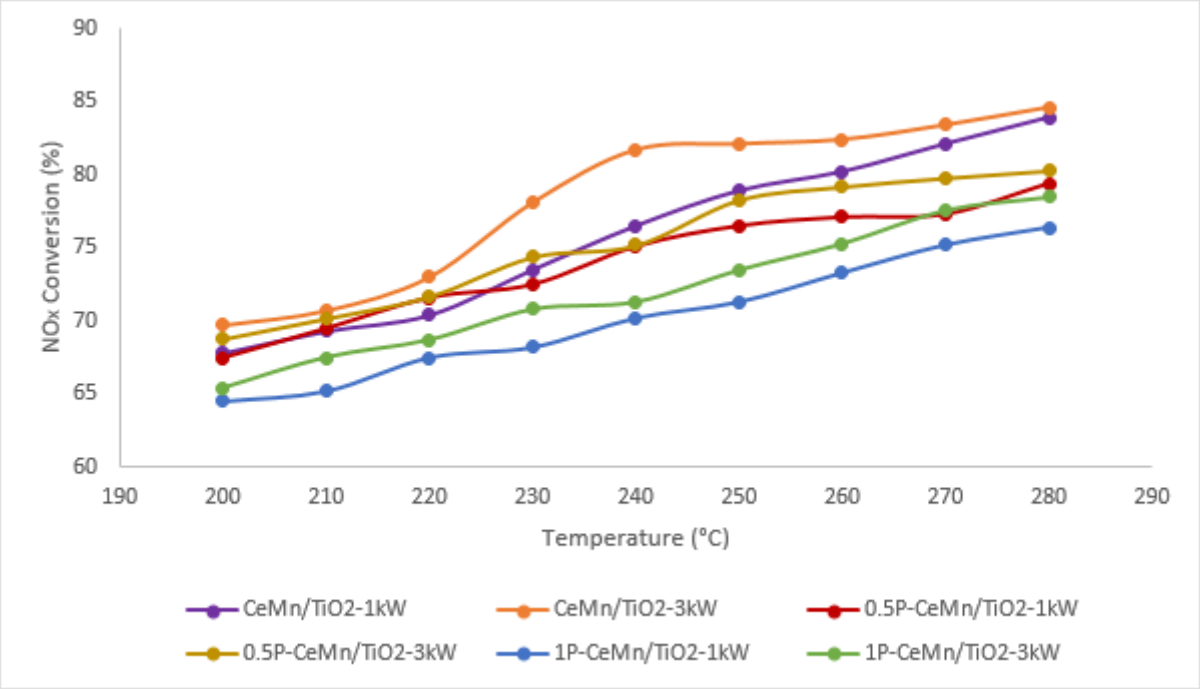

Figure 2

NOx conversions of catalysts at 1 kW and 3 kW engine loads

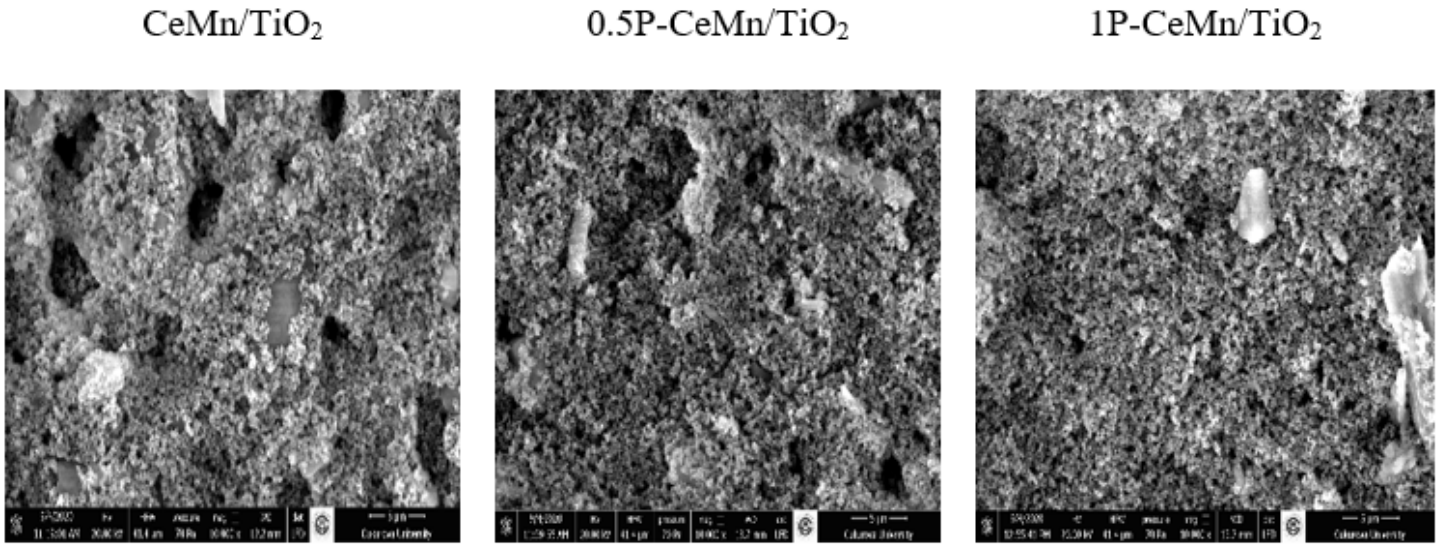

Figure 3

SEM images of CeMn/TiO2, 0.5P-CeMn/TiO2 and 1P-CeMn/TiO2 catalysts

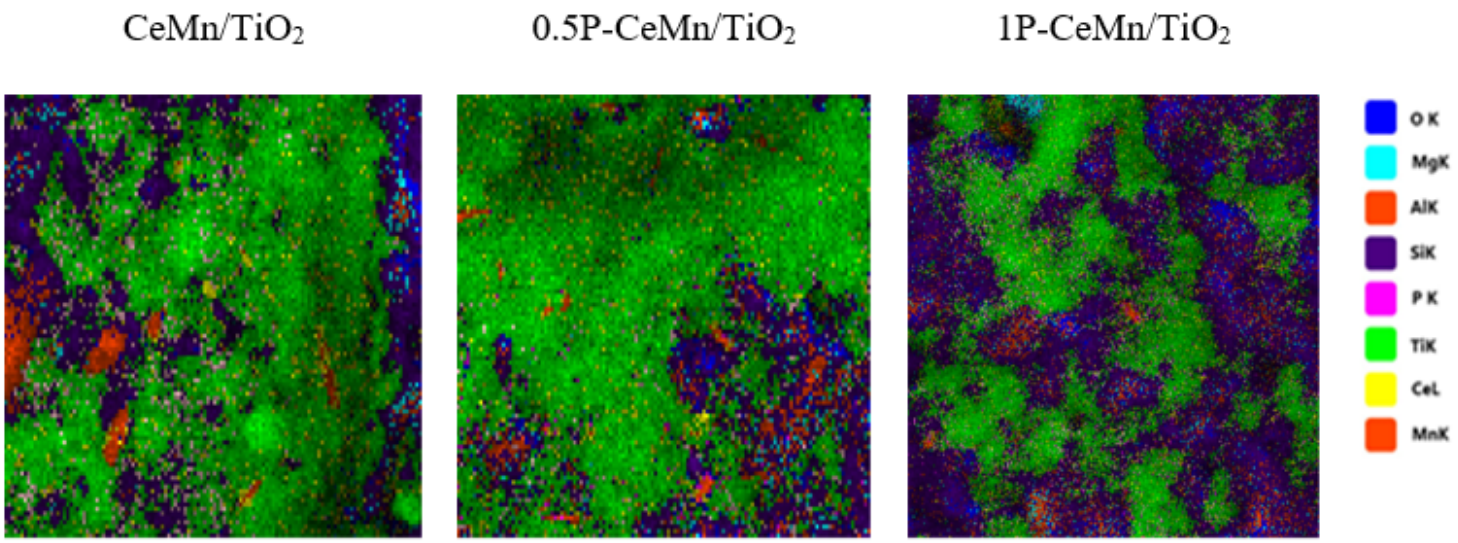

Figure 4

EDX mappings of CeMn/TiO2, 0.5P-CeMn/TiO2 and 1P-CeMn/TiO2 catalysts

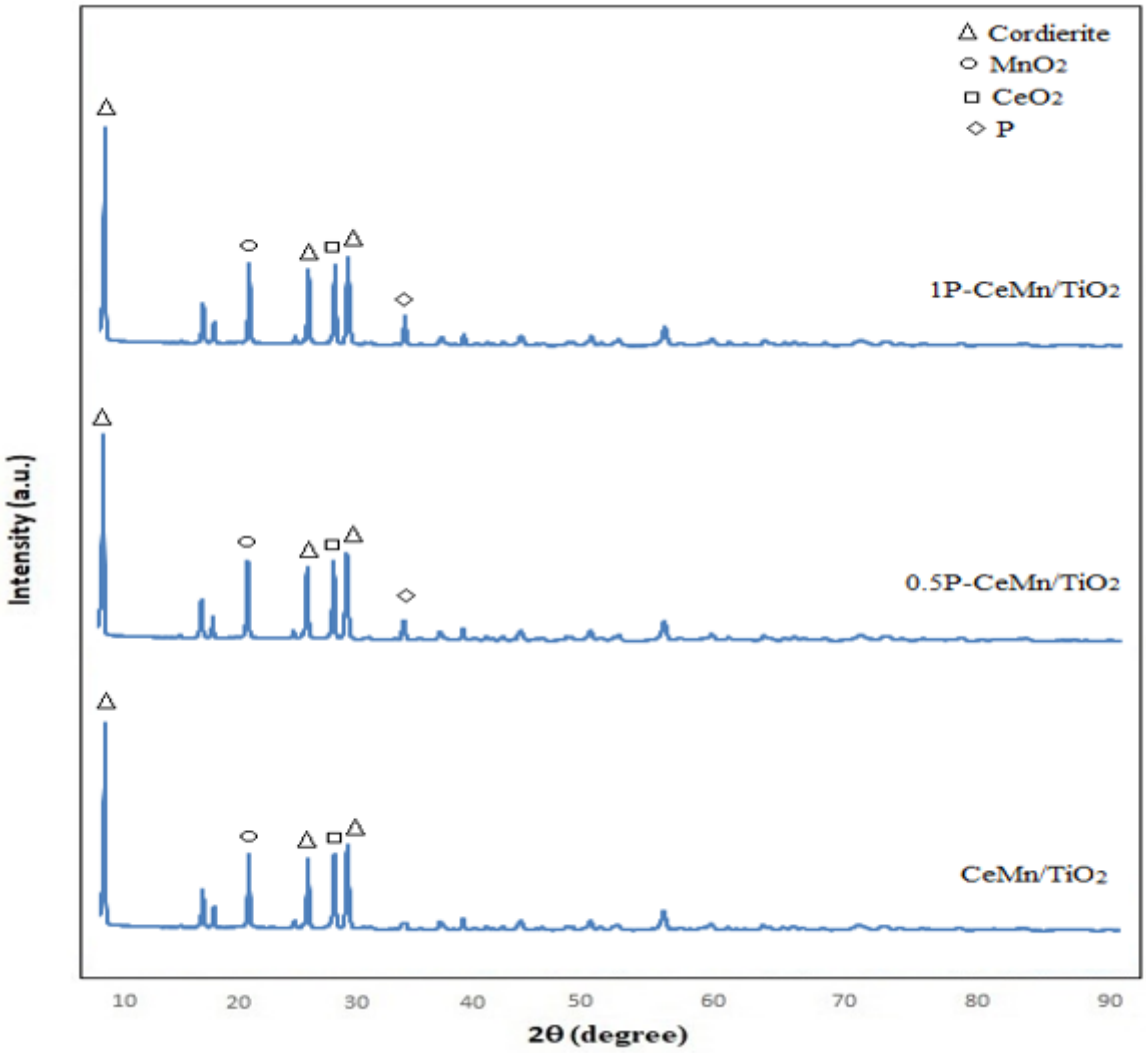

Figure 5

XRD patterns of CeMn/TiO2, 0.5P-CeMn/TiO2 and 1P-CeMn/TiO2 catalysts

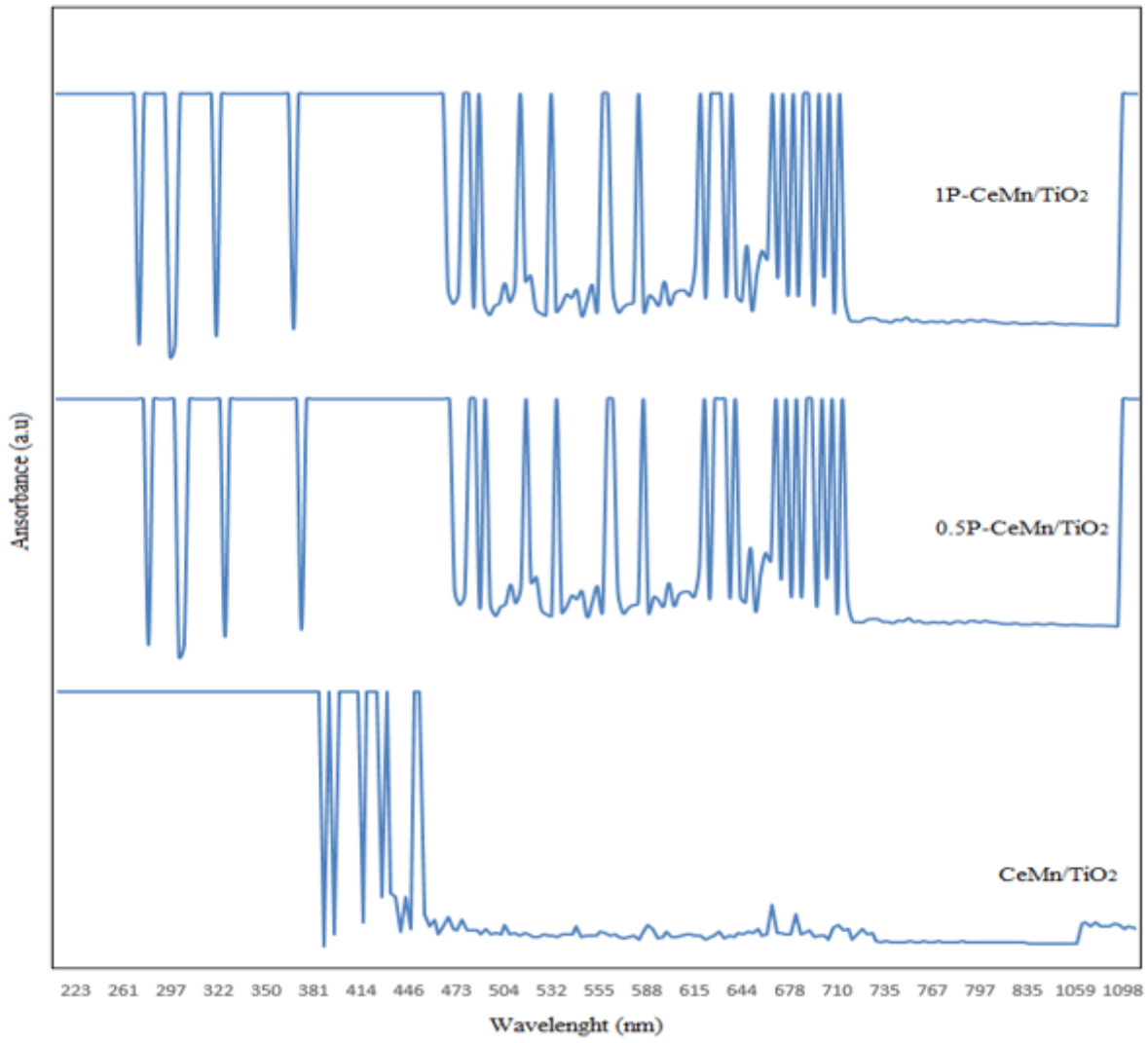

Figure 6

UV-Vis spectra of CeMn/TiO2, 0.5P-CeMn/TiO2 and 1P-CeMn/TiO2 catalysts